Model-Based Dynamic Sliding Mode Control and Adaptive Kalman Filter Design for Boiler-Turbine Energy Conversion System

Article in Journal of Process Control · July 2022

DOI: 10.1016/j.jprocont.2022.06.006

5 authors, including:

Imtiaz Ur Rehman
COMSATS University Islamabad

Syed Bilal Javed
National Engineering & Scientific Commission, Islamabad, Pakistan

Afraz Mehmood Chaudhry
Capital University of Science & Technology

Rizwan Azam
COMSATS University Islamabad

Model-Based Dynamic Sliding Mode Control and Adaptive Kalman Filter Design for Boiler-Turbine Energy Conversion System

Imtiaz Ur Rehman[a], Syed Bilal Javed[a], Afraz Mehmood Chaudhry[b], Muhammad Rizwan Azam[a], Ali Arshad Uppal[a,*]

[a] *Department of Electrical and Computer Engineering, COMSATS University Islamabad, Islamabad, Pakistan*
[b] *Department of Engineering Technology, Vrije Universiteit Brussel*

Abstract

The model-based control of a boiler-turbine system (BTS) is a formidable task due to coupling in state variables, nonlinearities and constraints on the control inputs. In this paper, a model-based, multi-variable dynamic sliding mode control (DSMC) is designed for the nonlinear BTS model to maintain the drum pressure, electric power and water level at the desired levels. In DSMC, an implicit sliding manifold is designed for the water level due to its complexity and explicit dependence on the control inputs. For this purpose, an auxiliary function is computed, and the sliding mode is enforced in such a way that the system fluid density tracks the auxiliary function, and subsequently the water level tracks the desired trajectory. Owing to its complexity, the time derivative of the auxiliary function is computed using the uniform robust exact differentiator (URED). An adaptive Kalman filter (AKF) is designed for the estimation of the unmeasurable state i.e., system fluid density. The design of AKF is based on the quasi-linear model of the BTS. Furthermore, a detailed stability analysis is carried out to ensure the boundedness of the closed-loop system. The simulation results depict that the designed control scheme exhibits the desired tracking performance in the presence of external disturbances, nonlinearities, constraints on the inputs, and measurement and process noises.

*A. A. Uppal
Email address: ali_arshad@comsats.edu.pk (Ali Arshad Uppal)

Keywords:
Boiler-turbine system (BTS), Multi-variable dynamic sliding mode control (DSMC), Adaptive Kalman filter (AKF), Energy conversion systems

1. Introduction

A boiler-turbine system (BTS) is a critical component of an electric power plant. There are two levels of energy conversion in a BTS, initially chemical energy is converted into mechanical energy, which is further converted into electrical energy, cf. [1, 2]. The primary function of a BTS is to meet the electricity demand while keeping the drum pressure, electric power and water level within the specified limits regardless of the load variations, cf. [3]. At the beginning of the BTS operation, water enters into the economizer section before getting into the steam drum. The economizer transfers the heat of boiler stack gases to the boiler feed water and raises its temperature. The main function of the steam drum is to separate water and steam coming from the economizer and water walls, respectively. The steam generated in the steam drum is provided to the inlets of high and low-pressure turbines to generate electricity. The steam is super-heated to a high temperature before entering the turbines, cf. [1, 4].

The Researchers have been extensively working on the modeling and control of BTS for the last three decades. The control system design of a BTS has a significant importance to achieve the desired performance and for the safe operation of a power plant. However, the development of a control system for a BTS is a challenging task due to the process nonlinearities, external disturbances, strong coupling between state variables and inputs, and physical limitations imposed on the control inputs, cf. [1, 5, 6].

1.1. Related Work

Over the years, numerous linear and nonlinear control techniques have been designed for the BTS to achieve the desired levels of the output power, drum pressure and water by manipulating the flow rate of fuel, steam and water, respectively. In [2, 7–10], various linear controllers are designed by linearizing the nonlinear BTS model reported in [11]. Tan et al, cf. [2, 9] have designed loop shaping design based H_∞ and PID controllers for the BTS. The controllers exhibit good tracking performance in the presence of modeling inaccuracies. However, the conventional PID controller is not optimal for

BTS due to hard nonlinearities, cf. [1]. In [7], the nonlinear BTS model proposed in [11] is transformed into the linear parameter varying (LPV) form to design the gain scheduled controller. The simulation results show that the desired performance is achieved. In [8], Dimeno and Lee have designed PI and state feedback controllers by using the genetic algorithm (GA). The external disturbances are not considered in the control design. The results of both the controllers are compared, which show the superiority of state feedback control law. In [10], authors have linearized the BTS model proposed in [11] to design the H_∞ controller. The simulation results show the adequate performance of the designed controller both in the time and frequency domains.

In [6, 12–23], the model proposed in [11] is employed to design various model-based nonlinear control techniques. In [6], the BTS model is simplified to design the disturbance rejection control (DRC) and the unknown states and external disturbances are also estimated by designing a higher order sliding mode observer (SMO). However, large control efforts and a slight deterioration in output tracking are observed due to model simplification. In [12], authors have designed the robust adaptive sliding mode control (RASMC) using the input-output feedback linearization procedure. Moreover, the type-I servo controller is designed by linearizing the BTS model around a single operating point. Both the control schemes are implemented on the nonlinear model and the simulation results show the superiority of RASMC. Ghabraei et al, cf. [13] have designed the robust adaptive variable structure control (RAVSC) and H_∞ controller for the BTS. The RAVSC is designed by employing almost similar methodology presented in [12]. Both the controllers are implemented on the nonlinear model and the results depict that RAVSC has slightly better performance than H_∞ controller. In [14, 15], sliding mode control (SMC) is designed for the linear model proposed in [24] and [25], respectively. The results are also compared with the H_∞ controller and it is observed that the SMC outperforms H_∞. Ataei et al, cf. [16] have designed the SMC for the reduced order nonlinear model presented in [26]. The results of SMC are compared with PI controller which show the superiority of SMC.

Similarly, authors have used the feedback linearization and gain scheduling techniques to design the control laws for BTS, cf. [17]. The simulation results illustrate that the control design based on feedback linearization gives better performance as compared to gain-scheduling controller. In [18], the model proposed in [26] is used to design the decentralized control by employing the backstepping technique. The model is partitioned into two sub-systems and the control laws are designed separately for each sub-system.

The desired levels of the throttle pressure and output power are maintained by manipulating the throttle valve position and firing rate. In [19–22], fuzzy sliding mode control (FSMC), nonlinear predictive control (NPC), robust model predictive control (RMPC) and general active disturbance rejection control (GADRC) are designed, respectively by linearizing the BTS model presented in [11]. In [19], authors have designed the FSMC to eliminate the chattering phenomenon in the conventional SMC. Moreover, the results of PI control and SMC are compared with FSMC which show the predominancy of FSMC. In [20], the extended kalman filter (EKF) is also used to estimate the unknown states. In [21], authors have constructed a global LPV model by combining the linearized models obtained at various operating points. Zhu et al. [22] have designed the multivariable extended state observer (MESO) for the estimation of external disturbances. The results are compared with H_∞ and model predictive control with integral action (MPC-integral), which shows better performance of GADRC. Lei et al, cf. [23] have linearized the BTS model presented in [27] to designed the internal model robust adaptive control (IMRAC). Moreover, authors have designed the state predictor for the unmeasurable state used in the control design. The IMRAC is compared with fuzzy extended state observer based predictive control which shows the supremacy of the designed control law. To identify the gap analysis, the related work of nonlinear control techniques is summarized in Table 1.

1.2. Gap Analysis

In our previous work, cf. [28] the super-twisting based SMC is designed for the drum boiler system (DBS). The decentralized control law is designed based on the assumption that u_1 and u_2 have a significant impact on y_1 and y_2, respectively. However, the decentralized controller is not feasible for the BTS due to its highly coupled nature. It is evident in the above-mentioned literature that mostly nonlinear control techniques are designed by assuming that the system fluid density is directly measurable. However, it is highly unrealistic to design the model-based control by using the unmeasurable states, cf. [6, 29–33]. Hence, the estimator design is essential to develop a control system for the BTS. It is also pertinent to mention that the mathematical expression for the water level, one of the outputs of the BTS, is highly nonlinear and complex. Moreover, the water level has an explicit dependence on the control inputs which further complicates the design of SMC. Therefore, the direct control of water level is quite cumbersome. Most of the literature focuses on the control of drum pressure, electrical power and system

Table 1: Notable contributions for the control of BTS

Control Techniques	**Year**	**Model Type**	**Major simplifications**	**Linearization Technique**	**State Estimator Design**	**Implementation considerations**			
						Nonlinear model	**Disturbances**	**Process noise**	**Measurement noise**
RMPC [21]	2021		Linearization	TSE	✗	✓	✓	✗	✗
IMRAC [23]	2020		Linearization	TSE	State predictor	✓	✓	✗	✗
GADRC [22]	2019	Nonlinear	Linearization	TSE	✗	✓	✓	✗	✗
DRC [6]	2018		Assumed complex terms in y_3 as disturbance	✗	✗	✓	✓	✗	✓
RAVSC [13]	2018		Assumed y_3=x_3	Input-Output	✗	✓	✓	✗	✗
NPC [20]	2017		Linearization	TSE	EKF	✓	✓	✓	✓
RASMC [12]	2015		Assumed y_3=x_3	Input-Output	✗	✓	✓	✗	✗
SMC [16]	2014		Reduced order model	✗	✗	✓	✓	✗	✗
FSMC [19]	2013		Linearization	TSE	✗	✗	✓	✗	✗
SMC [15]	2012	LTV	✗	✗	✗	✗	✓	✗	✗
BBC [18]	2011	Nonlinear	Decentralized controller	✗	✗	✓	✓	✗	✗
SMC [14]	2009	LTI	✗	✗	✗	✗	✓	✗	✗

LTI= Linear time invariant; LTV= Linear time variant; TSE= Taylor series expansion
x_3= system fluid density; y_3= water level

fluid density pertaining to a BTS. Furthermore, the BTS model is linearized through Taylor series expansion (TSE) for both the observer and controller designs. The linearization of highly nonlinear systems by TSE can cause instability [34–36]. Moreover, the control design based on the linear model always ensure adequate performance and stability for a limited operating range. Thus, the design of a centralized control law based on the nonlinear model along with a state estimator is essential for the BTS to address the aforesaid shortcomings.

1.3. Major Contributions

As described in the gap analysis, BTS is a highly coupled nonlinear system, therefore, it is not possible to figure out which output is affected by which input. Hence, practically for such systems centralized controller is a perfect choice instead of a decentralized controller to achieve the desired performance. Thus, in this work, a nonlinear model-based centralized dynamic sliding mode control (DSMC) is designed to maintain the drum pressure, electric power and water level at the desired levels. The primary reason to design a DSMC is to mitigate the chattering phenomena which inherently exists in a conventional SMC. In the literature, the design of numerous control laws are based on the assumption that the system's fluid density is available. However, in practice, this state is not directly measurable, and it is impractical to use it directly in the model-based control. For this purpose, an adaptive Kalman filter (AKF) is designed which adapts initial biased covariances to provide an accurate estimate the system fluid density of the BTS. DSMC is designed in such a way that the sliding mode is established in a manifold where the system fluid density attains the desired level, which is chosen in such a way that the water level follows its reference trajectory. In the gap analysis, it is also highlighted that the implementation scheme of the designed control laws is simplified by ignoring the process and measurement noises. In the proposed work, the designed control law is implemented on the nonlinear model with practical considerations like external disturbances, measurement and process noises.

The rest of the paper is organized as follows. The control-oriented model of the BTS is explained in Section 2, the problem statement is described in Section 3. The DSMC design and stability analysis is presented in Section 4. The design of AKF is discussed in Section 5. The simulation results are presented in Section 6 and finally, this article is concluded in Section 7.

2. Model description

A suitable model selection has a significant role in the model-based control design. In the literature, various mathematical models of BTS have been proposed by the researchers, cf. [11, 27, 37–39]. The mathematical model of BTS proposed by Astrom and Bell, cf. [11] is employed to design the model-based control system. The mathematical model of the BTS proposed in (1) is a first principle based model, and it provides essential physical insight about the process. This model is simple and involves lesser number of parameters as compared to other models reported in the literature. Moreover, the model is extensively used in the literature for the BTS control design. The model equations are given as

$$
\begin{aligned}
\dot{x}_1 &= -a_{11}u_2x_1^{9/8} + a_{12}u_1 - a_{13}u_3 + d_1 + n_{p1}, \\
\dot{x}_2 &= (a_{21}u_2 - a_{22})x_1^{9/8} - a_{23}x_2 + d_2 + n_{p2}, \\
\dot{x}_3 &= \frac{[a_{31}u_3 - (a_{32}u_2 - a_{33})x_1]}{a_{34}} + d_3 + n_{p3},
\end{aligned} \tag{1}
$$

where $\mathbf{x} \in \Re^{3\times1}$, $\mathbf{u} \in \Re^{3\times1}$, $\mathbf{n_p} \in \Re^{3\times1}$, $\mathbf{d} \in \Re^{3\times1}$ and a_{ij} represent states, normalized inputs, process noises, unknown input disturbances and model parameters, respectively. The outputs are

$$
\begin{aligned}
y_1 &= x_1 + n_{m1}, \\
y_2 &= x_2 + n_{m2}, \\
y_3 &= a_{41}(a_{42}x_3 + a_{43}\alpha_{cs} + \frac{q_e}{a_{44}} - a_{45}) + n_{m3},
\end{aligned} \tag{2}
$$

where $\mathbf{n_m} \in \Re^{3\times1}$, α_{cs} and q_e are the measurement noises, steam quality and evaporation rate (kg/sec), respectively. The expressions for α_{cs} and q_e are given as

$$
\begin{aligned}
\alpha_{cs} &= \frac{(1 - a_{46}x_3)(a_{47}x_1 - a_{48})}{x_3(a_{49} - a_{50}x_1)}, \\
q_e &= (a_{51}u_2 - a_{52})x_1 + a_{53}u_1 - a_{54}u_3 - a_{55}.
\end{aligned}
$$

The states, the inputs and the outputs are summarized in Table 2, whereas, the model parameters are described in Table 3. The constraints on the inputs and their time derivatives describe the physical constraints on the actuators, cf. [11], and are given as

$$
\begin{aligned}
0 \leq u_{1,2,3} &\leq 1, \\
-0.007 \leq \dot{u}_1 &\leq 0.007, \\
-2 \leq \dot{u}_2 &\leq 0.02, \\
-0.05 \leq \dot{u}_3 &\leq 0.05.
\end{aligned} \tag{3}
$$

Table 2: List of symbols

Symbol	Description	Units
x_1	Drum pressure	kg/cm^2
x_2	Electric power	MW
x_3	System fluid density	kg/m^3
y_1	Drum pressure	kg/cm^2
y_2	Electric power	MW
y_3	Water level	m
u_1	Fuel flow rate	—
u_2	Steam flow rate	—
u_3	Water flow rate	—

Table 3: Nominal model parameters

a_{11}=0.0018	a_{12}=0.9	a_{13}=0.15
a_{21}=0.073	a_{22}=0.016	a_{23}=0.1
a_{31}=141	a_{32}=1.1	a_{33}=0.19
a_{34}=85	a_{41}=0.05	a_{42}=0.13073
a_{43}=100	a_{44}=9	a_{45}=67.975
a_{46}=0.001538	a_{47}=0.8	a_{48}=25.6
a_{49}=1.0394	a_{50}=0.00123404	a_{51}=0.854
a_{52}=0.147	a_{53}=45.59	a_{54}=2.514
a_{55}=2.096		

3. Problem Statement

To design a model-based nonlinear controller for BTS which drags the drum pressure, electric power and water level to the desired set points. The controller should be capable to ensure fast convergence, robustness and stability in the presence of external disturbances, and process and measurement noises. Also, the controller should meet the physical constraints imposed on the actuators.

4. Control Design

Owing to highly coupled states and inputs, a model-based, centralised DSMC is designed for the BTS by using the nonlinear model presented in

(1) and (2). The step by step design procedure of DSMC is summarize as follows:

1. The sliding variable vector $\sigma = \begin{bmatrix}\sigma_1 & \sigma_2 & \sigma_3\end{bmatrix}^T$ is selected such that the sliding mode shows the desired characteristics.
2. For obtaining continuous control input, a DSMC is designed by intentionally adding an integrator to enforce sliding mode in the time-derivative of the control input.
3. It can be seen in (2) that y_3 has a relative degree 0 with respect to all the control inputs. Therefore, enforcing the conventional sliding mode, i.e., $y_3 \rightarrow r_3$ through the sliding variables in (4) can render discontinuous terms in the right hand side of y_3, cf. (2). Hence, in order to avoid discontinuity and to obtain consistency in the relative degree, the sliding mode is enforced such that $x_3 \rightarrow x_{3f}$, where x_{3f} is an auxiliary function of the states and selected such that $y_3 \rightarrow r_3$.
4. For controller synthesis $\dot{x}_{3f}$ is also required. In order to avoid complex mathematical computations, $\dot{x}_{3f}$ is numerically obtained by uniform robust exact differentiator (URED) of [40]
5. A detailed stability analysis is carried out to prove that the closed-loop system is stable, even in the presence of modeling imperfections and external disturbances. Moreover, the maximum bounds of the allowable disturbances are also computed.

4.1. Dynamic Sliding Mode Control design

The vector of sliding variables is chosen to achieve the desired levels of drum pressure, electric power and water level. The sliding variables σ_i are selected as

$$\sigma_{\mathbf{i}} = \dot{\mathbf{e}}_i + \lambda_i \mathbf{e}_{\mathbf{i}}, \quad i = 1, 2, 3, \tag{4}$$

where $e_1 = y_1 - r_1$, $e_2 = y_2 - r_2$, $e_3 = x_3 - x_{3f}$ and $\lambda_i \in \Re^+$ are the design parameters. While, r_1 and r_2 are the desired levels of drum pressure and electric power respectively. The auxiliary function x_{3f} is computed by solving the third equation in (2) with $y_3 = r_3$, which yields the following quadratic equation

$$\varphi x_{3f}^2 + \beta x_{3f} + \gamma = 0, \tag{5}$$

where r_3 is the desired water level and the parameters φ, β and γ are expressed as follows

$$
\begin{aligned}
\varphi &= a_{41}a_{42},\\
\beta &= -r_3 - a_{41}a_{45} - \left(\frac{a_{41}a_{43}a_{46}(a_{47}x_1 - a_{48})}{(a_{49} - a_{50}x_1)}\right)\\
&\quad + \left(\frac{a_{41}}{a_{44}}x_1(a_{51}u_2 - a_{52}) + a_{53}u_1 - a_{54}u_3 - a_{55}\right),\\
\gamma &= \frac{a_{41}a_{43}(a_{47}x_1 - a_{48})}{(a_{49} - a_{50}x_1)}.
\end{aligned}
$$

The solution of (5) is given as

$$
x_{3f} = \frac{-\beta \pm \sqrt{\beta^2 - 4\varphi\gamma}}{2\varphi}.
$$

Depending on the values of the model parameters, cf. Table 3, both values of x_{3f} are positive, real and distinct. By consulting the literature, we have opted for the higher value of x_{3f}. The time derivatives of errors and σ are determined as follow

$$
\begin{bmatrix}\dot{e}_1\\ \dot{e}_2\\ \dot{e}_3\end{bmatrix} = \begin{bmatrix} a_{12} & a_{11}x_1^{9/8} & -a_{13}\\ 0 & a_{21}x_1^{9/8} & 0\\ 0 & -\frac{a_{32}}{a_{34}}x_1 & \frac{a_{31}}{a_{34}}\end{bmatrix}\begin{bmatrix}u_1\\ u_2\\ u_3\end{bmatrix} - \begin{bmatrix}\dot{r}_1\\ \dot{r}_2 + a_{22})x_1^{9/8} + a_{23}x_2\\ \dot{x}_{3f} - \frac{a_{33}}{a_{34}}x_1\end{bmatrix}, \tag{6}
$$

$$
\begin{aligned}
\begin{bmatrix}\dot{\sigma}_1\\ \dot{\sigma}_2\\ \dot{\sigma}_3\end{bmatrix} &= \begin{bmatrix} -\frac{9}{8}a_{11}u_2x_1^{1/8} + \lambda_1 & 0 & 0\\ \frac{9}{8}x_1^{1/8}(a_{21}u_2 - a_{22}) & -a_{23} + \lambda_2 & 0\\ \frac{[(a_{33} - a_{32}u_2)]}{a_{34}} & 0 & \lambda_3\end{bmatrix}\begin{bmatrix}\dot{x}_1\\ \dot{x}_2\\ \dot{x}_3\end{bmatrix} + \begin{bmatrix}\lambda_1 d_1 + \dot{d}_1\\ \lambda_2 d_2 + \dot{d}_2\\ \lambda_3 d_3 + \dot{d}_3\end{bmatrix}\\
&\quad + \begin{bmatrix} a_{12} & -a_{11}x_1^{9/8} & -a_{13}\\ 0 & a_{21}x_1^{9/8} & 0\\ 0 & -\frac{a_{32}}{a_{34}}x_1 & \frac{a_{31}}{a_{34}}\end{bmatrix}\begin{bmatrix}\dot{u}_1\\ \dot{u}_2\\ \dot{u}_3\end{bmatrix} - \begin{bmatrix}\lambda_1\dot{r}_1 + \ddot{r}_1\\ \lambda_2\dot{r}_2 + \ddot{r}_2\\ \lambda_3\dot{x}_{3f} + \ddot{x}_{3f}\end{bmatrix}.
\end{aligned} \tag{7}
$$

The unknown disturbances ($\mathbf{d} = \begin{bmatrix} d_1 & d_2 & d_3\end{bmatrix}^T$) are assumed norm-bounded in C^1, i.e. $|\mathbf{d}(\mathbf{t})| \leq \rho$, where ρ is unknown for the controller. The computation of time derivatives of x_{3f} is a formidable task due to its high complexity. For this purpose, the uniform robust exact differentiator (URED) is employed. The error (Θ) between input (x_{3f}) and the estimated ($\hat{x}_{3f}$) signal is given as

$$\Theta = x_{3f} - \hat{x}_{3f}. \tag{8}$$

Now by using the super twisting algorithm (STA), the time derivatives of the estimated signal are

$$\begin{aligned} \dot{\hat{x}}_{3f} &= -\digamma_1 \Pi_1(\Theta) + \hat{\dot{x}}_{3f}, \\ \dot{\hat{\dot{x}}}_{3f} &= -\digamma_2 \Pi_2(\Theta), \end{aligned} \tag{9}$$

where $\digamma_1, \digamma_2 \in R^+$. The functions $\Pi_1(\Theta)$ and $\Pi_2(\Theta)$ are given below.

$$\begin{aligned} \Pi_1(\Theta) &= |\Theta|^{\frac{1}{2}} \operatorname{sgn}(\Theta) + \mu |\Theta|^{\frac{3}{2}} \operatorname{sgn}(\Theta), \\ \Pi_2(\Theta) &= \frac{1}{2} \operatorname{sgn}(\Theta) + 2\mu\Theta + \frac{3}{2}\mu^2 |\Theta|^2 \operatorname{sgn}(\Theta), \end{aligned} \tag{10}$$

where $\mu \geq 0$ is a scalar, and the terms $|\Theta|^{\frac{3}{2}} \operatorname{sgn}(\Theta)$ and $|\Theta|^2 \operatorname{sgn}(\Theta)$ give uniform convergence irrespective of the initial conditions of the differentiator [40]. Similarly $\ddot{x}_{3f}$ is also computed using the same procedure. The continuous part of the control input $\mathbf{v_{eq}} = \dot{\mathbf{u}}_{\mathbf{eq}} = [v_{eq1}, v_{eq2}, v_{eq3}]^T$ is computed by solving $\dot{\sigma} = 0$. Thus, the equivalent control is

$$\begin{bmatrix} v_{eq_1} \\ v_{eq_2} \\ v_{eq_3} \end{bmatrix} = \begin{bmatrix} a_{12} & -a_{11}x_1^{9/8} & -a_{13} \\ 0 & a_{21}x_1^{9/8} & 0 \\ 0 & -\frac{a_{32}}{a_{34}}x_1 & \frac{a_{31}}{a_{34}} \end{bmatrix}^{-1} \left(\begin{bmatrix} \lambda_1 \dot{r}_1 + \ddot{r}_1 \\ \lambda_2 \dot{r}_2 + \ddot{r}_2 \\ \lambda_3 \dot{x}_{3f} + \ddot{x}_{3f} \end{bmatrix} \right.$$
$$\left. + \begin{bmatrix} \frac{9}{8}a_{11}u_2 x_1^{1/8} - \lambda_1 & 0 & 0 \\ -\frac{9}{8}x_1^{1/8}(a_{21}u_2 - a_{22}) & a_{23} - \lambda_2 & 0 \\ -\frac{[(a_{33} - a_{32}u_2)]}{a_{34}} & 0 & -\lambda_3 \end{bmatrix} \begin{bmatrix} \dot{x}_1 \\ \dot{x}_2 \\ \dot{x}_3 \end{bmatrix} \right),$$

and the above expression can be written as

$$\mathbf{v_{eq}} = B^{-1}F. \tag{11}$$

Hence, the overall DSMC control law becomes

$$\dot{\mathbf{u}} = B^{-1}F - Nsgn(\sigma), \tag{12}$$

where $N = \begin{bmatrix} N_1 & 0 & 0 \\ 0 & N_2 & 0 \\ 0 & 0 & N_3 \end{bmatrix}$ and $N_1, N_2, N_3 \in \Re^+$.

The controller in (12) is called the dynamic SMC because the discontinuous term is introduced in the time derivative of the control input. Consequently, (12) is integrated to yield the control input.

4.2. Stability Analysis

To be able to use a Lyapunov function to determine the stability conditions of the sliding mode, the control components in (7) are replaced with the corresponding expressions found in (12), yielding

$$\underbrace{\begin{bmatrix} \dot{\sigma}_1 \\ \dot{\sigma}_2 \\ \dot{\sigma}_3 \end{bmatrix}}_{\dot{\sigma}} = -\underbrace{\begin{bmatrix} a_{12}N_1 & -a_{11}x_1^{9/8}N_2 & -a_{13}N_3 \\ 0 & a_{21}x_1^{9/8}N_2 & 0 \\ 0 & -\frac{a_{32}}{a_{34}}x_1N_2 & \frac{a_{31}}{a_{34}}N_3 \end{bmatrix}}_{D(x)} \underbrace{\begin{bmatrix} sgn(\sigma_1) \\ sgn(\sigma_2) \\ sgn(\sigma_3) \end{bmatrix}}_{sgn(\sigma)} + \underbrace{\begin{bmatrix} \lambda_1 d_1 + \dot{d}_1 \\ \lambda_2 d_2 + \dot{d}_2 \\ \lambda_3 d_3 + \dot{d}_3 \end{bmatrix}}_{\tilde{d}}. \tag{13}$$

The above equation can also be presented in a compact form as

$$\dot{\sigma} = -D(x)\,\mathrm{sgn}(\sigma) + \tilde{d}. \tag{14}$$

To prove the convergence of the sliding mode, a Lyapunov function of the form stated below is chosen

$$V = |\sigma_1| + |\sigma_2| + |\sigma_3|\,, \tag{15}$$

The time derivative of the above Lyapunov function is calculated to be

$$\begin{aligned} \dot{V} &= \frac{\partial V}{\partial \sigma_1}\dot{\sigma}_1 + \frac{\partial V}{\partial \sigma_2}\dot{\sigma}_2 + \frac{\partial V}{\partial \sigma_3}\dot{\sigma}_3, \\ &= \frac{\sigma_1}{|\sigma_1|}\dot{\sigma}_1 + \frac{\sigma_2}{|\sigma_2|}\dot{\sigma}_2 + \frac{\sigma_3}{|\sigma_3|}\dot{\sigma}_3, \\ &= \mathrm{sgn}\,(\sigma_1)\dot{\sigma}_1 + \mathrm{sgn}\,(\sigma_2)\dot{\sigma}_2 + \mathrm{sgn}\,(\sigma_3)\dot{\sigma}_3. \end{aligned} \tag{16}$$

The above equation can also be written in a compact form as

$$\dot{V} = \mathrm{sgn}^T(\sigma)\dot{\sigma}. \tag{17}$$

The convergence conditions for the nominal system and the perturbed system are presented separately in the subsequent sections.

4.2.1. Stability of Nominal System

For the nominal system, the disturbance term $\tilde{d}$ in (14) is eliminated. Therefore, the time derivative of the sliding variable for the nominal system is represented as

$$\dot{\sigma} = -D(x)\,\mathrm{sgn}(\sigma). \tag{18}$$

According to [41], for $\dot{\sigma}$ written in the above form, if the matrix D is positive definite, then the origin is a finite time stable equilibrium point. The matrix D, presented in (13) can be proven to be positive definite if all of its leading principal minors M_{ij}, are positive:

$$\begin{aligned} M_{11} &= \frac{a_{31}}{a_{34}}N_3, \\ M_{22} &= \frac{a_{12}a_{31}}{a_{34}}x_1^{9/8}N_2N_3, \\ M_{33} &= \frac{a_{12}^2a_{31}}{a_{34}}x_1^{9/8}N_1N_2N_3. \end{aligned} \tag{19}$$

Since all the components N_i, a_{ij} and $x_i \in \Re^+$, hence, all the principal minors in (19) are positive. Therefore, the matrix D is positive definite and hence it is proved that the origin $\sigma = 0$ is a finite time stable equilibrium point.

4.2.2. Stability of Perturbed System

The results of nominal stability can be extended for the perturbed system defined in (13). For $\sigma(x) = 0$ to be a sliding manifold, it is sufficient that matrix D is positive definite and

$$\begin{gathered} \lambda_0 > \tilde{d}_0\sqrt{m} \;\; with \;\; \lambda_{min}(x) > \lambda_0 > 0, \\ \|\tilde{d}(t)\| < \tilde{d}_0, \end{gathered} \tag{20}$$

where m is the number of inputs, $\lambda_0 \in \Re^+$, $\tilde{d}_0$ is the upper bound of vector $\tilde{d}$ defined in (14), and $\lambda_{min}(x)$ is the minimum eigenvalue of $\frac{D+D^T}{2}$. Then the time derivative of Lyapunov function will be of the form

$$\dot{V}(t) \leq \tilde{d}_0\sqrt{m} \, - \, \lambda_0 < 0. \tag{21}$$

The upper bound of the disturbance vector $\tilde{d}(t)$ and hence the value of $\tilde{d}_0$ are computed analytically is known. The design parameters of sliding mode in (4) are chosen as $\lambda_1 = 0.02$, $\lambda_2 = 0.2$ and $\lambda_3 = 0.1$. The profiles of the disturbances given in [12] are selected to evaluate the robustness of the proposed control scheme

$$\begin{aligned} d_1(t) &= 30 \times 10^{-4} \;\cos(0.5t), \\ d_2(t) &= 30 \times 10^{-4} \;\cos(0.5t), \\ d_3(t) &= 30 \times 10^{-4} \;\cos(0.75t). \end{aligned} \tag{22}$$

By replacing the values of λ_i and $d_i(t)$, the expressions for $\tilde{d}_i(t)$ becomes

$$\begin{aligned} \tilde{d}_1(t) &= 30 \times 10^{-4}\big(\lambda_1 \;\cos(0.5t) - 0.5 \;\sin(0.5t)\big), \\ \tilde{d}_2(t) &= 30 \times 10^{-4}\big(\lambda_2 \;\cos(0.5t) - 0.5 \;\sin(0.5t)\big), \\ \tilde{d}_3(t) &= 30 \times 10^{-4}\big(\lambda_3 \;\cos(0.75t) - 0.75 \;\sin(0.75t)\big). \end{aligned} \tag{23}$$

By considering the fact that the maximum value of trigonometric functions in (23) will be 1, the upper bound of $\tilde{d}$ is found to be

$$\tilde{d} = [-0.0014 \;\; -0.0009 \;\; -0.0020]^T, \tag{24}$$

and the norm of $\tilde{d}$ is calculated to be $\|\tilde{d}(t)\| = 0.0026$. Hence, according to the condition (20), $\tilde{d}_0 = 0.003$.

As the matrix D is state dependent, hence the right hand side of the inequality in (21) is evaluated numerically. It can be observed in Fig. 1 that (21) holds for the whole length of the simulations, therefore, $\sigma = 0$ is a sliding manifold and sliding mode occurs after a finite time interval, even for the perturbed system.

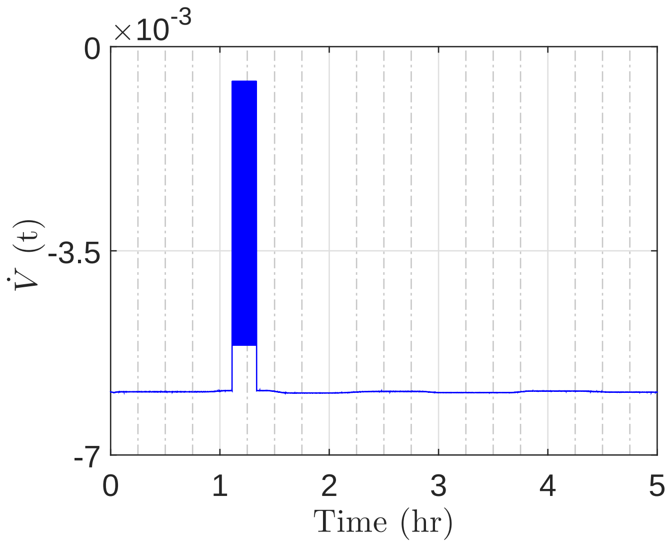

Figure 1: Time derivative of Lyapunov function.

5. Adaptive Kalman Filter Design

In order to make the model-based control design possible, the unknown state of BTS, i.e., x_3 needs to be estimated. Therefore, the AKF is designed to reconstruct x_3. The effect of process and measurement noises is also included in the system since the performance of the KF depends on sensor and process noise covariances [42]. Generally, in practical applications these covariances are partially known or completely unknown [42]. Hence, in order to improve the performance of KF, the initial biased unknown covariance matrices are adapted using AKF which works on the principle of extended Kalman filter (EKF). The filter adapts the unknown initial biased values of covariances through its adaptation rules and provides better estimates along with improved noise cancellation [42].

The nonlinear model of the BTS in (1) is first discretized and then decomposed using quasi-linear approach [43] in order to implement linear-discrete AKF framework, cf. [42]. The nonlinear model of the BTS in (1) can be written in a compact form as

$$\dot{x} = f(x) + b(x)u + d + n_p, \tag{25}$$

where $f, d, n_p \in R^3$ and $b \in R^{3x3}$ are characterized as

$$f(x) = \begin{bmatrix} 0 \\ -a_{22}x_1^{9/8} - a_{23}x_2 \\ \frac{a_{33}}{a_{34}}x_1 \end{bmatrix},$$
$$b(x) = \begin{bmatrix} a_{12} & -a_{11}x_1^{9/8} & -a_{13} \\ 0 & a_{21}x_1^{9/8} & 0 \\ 0 & -\frac{a_{32}}{a_{34}}x_1 & \frac{a_{31}}{a_{34}} \end{bmatrix}, d = \begin{bmatrix} d_1 \\ d_2 \\ d_3 \end{bmatrix}, n_p = \begin{bmatrix} n_{p1} \\ n_{p2} \\ n_{p3} \end{bmatrix}. \tag{26}$$

The model is discretized with a step size of $\Delta t = 0.01$ s, by using explicit Euler method, cf. [44]. The discrete nonlinear form of BTS is given as

$$x_{k+1} = x_k + f(x_k) + Bu(k) + D + N, \tag{27}$$

where $f(x_k) = \Delta t f(x(t))$, $B = \Delta tb$, $D = \Delta td$ and $N = \Delta tn_p$.

Similarly, the output y given in (2) can be written in compact and discrete form as

$$y_k = h(x_k) + l(x_k)u_k + \Omega + n_{mk}, \tag{28}$$

where $y_k \in \Re^3$, $h \in \Re^3, l \in \Re^{3\times3}$, $n_m \in \Re^3$ and constant vector $\Omega \in \Re^3$ are given as

$$h(x_k) = \begin{bmatrix} x_{1k} \\ x_{2k} \\ a_{41}\left(a_{42}x_{3k} + a_{43}(\frac{(1-a_{46}x_{3k})(a_{47}x_{1k}-a_{48})}{x_{3k}(a_{49}-a_{50}x_{1k})}) - \frac{a_{52}x_{1k}+a_{55}}{a_{44}} - a_{45}\right) \end{bmatrix},$$
$$l(x_k) = \begin{bmatrix} 0 & 0 & 0 \\ 0 & 0 & 0 \\ \frac{a_{41}a_{53}}{a_{44}} & \frac{a_{41}a_{51}}{a_{44}}x_{1k} & -\frac{a_{41}a_{54}}{a_{44}} \end{bmatrix},$$
$$\Omega = \begin{bmatrix} 0 \\ 0 \\ -(a_{41}a_{45} - \frac{a_{41}a_{55}}{a_{44}}) \end{bmatrix}, n_{mk} = \begin{bmatrix} n_{mk1} \\ n_{mk2} \\ n_{mk3} \end{bmatrix}. \tag{29}$$

In the second step, Eqs. (27) and (28) are decomposed using quasi-linear approach as proposed in [43] to have the following state-space representation, comprising of state dependent matrices

$$
\begin{aligned}
x_{k+1} &= A(x_k)\,x_k + B(x_k)u_k + D + n_{pk}, \\
y_k &= C(x_k)\,x_k + l(x_k)u_k + \Omega + n_{mk},
\end{aligned} \tag{30}
$$

where $A(x_k) \in \mathbb{R}^{3\times3}$, $B \in \mathbb{R}^{3\times1}$ and $C(x_k) \in \mathbb{R}^{3\times3}$. The state dependent matrices $A(x_k)$ and $C(x_k)$ correspond to the quasi-linear form of $f(x_k)$ and $h(x_k)$ given in Eqs. (26) and (29), respectively are given as

$$
\begin{aligned}
A(x_k) &= \begin{bmatrix} | & | & | \\ r_1 & r_2 & r_3 \\ | & | & | \end{bmatrix}, \\
C(x_k) &= \begin{bmatrix} | & | & | \\ c_1 & c_2 & c_3 \\ | & | & | \end{bmatrix}.
\end{aligned} \tag{31}
$$

The elements of $A(x_k)$ and $C(x_k)$ are obtained by using following expression as given in [43]

$$
r_k = \nabla f_k(x_k) + \frac{f_k(x_k) - x_k^T \nabla f_k(x_k)}{\|x_k\|^2} x_k, \qquad x_k \neq 0. \tag{32}
$$

$$
c_k = \nabla h_k(x_k) + \frac{h_k(x_k) - x_k^T \nabla h_k(x_k)}{||x_k||^2} x, \qquad x_k \neq 0, \tag{33}
$$

where $\nabla(.)$ is the gradient of a smooth vector field in the direction of state trajectories.

Now, AKF is designed for the following system

$$
\begin{aligned}
x_{k+1} &= A(x_k)\,x_k + B(x_k)u_k + D + n_{pk}, \\
y_k &= C(x_k)\,x_k + l(x_k)u_k + \Omega + n_{mk}, \\
&\quad n_{pk} \sim \mathcal{N}(0, Q_k), \\
&\quad n_{mk} \sim \mathcal{N}(0, R_k), \\
&\quad E[(n_{mk}\, n_{mk}^T)] = R_k \delta_{k-j}, \\
&\quad E[(n_{pk}\, n_{pk})] = Q_k \delta_{k-j}, \\
&\quad E[(n_{pk}\, n_{mk}^T)] = 0,
\end{aligned} \tag{34}
$$

where the kronecker delta function $\delta_{k-j} = 1$ if $k = j$ and $\delta_{k-j} = 0$ if $k \neq j$. Both process noise n_{pk} and sensor noise n_{mk} are white, zero mean, uncorrelated and with unknown covariance matrices $Q_k \in \mathbb{R}^{3\times 3}$ and $R_k \in \mathbb{R}^{3\times 3}$, respectively.

The idea behind AKF is to add two recursive unbiased updating rules for the measurement noise covariance R_k and process noise covariance Q_k. These rules are derived based on the covariance matching principle [42]. Also, updating rules have the ability to tune the noise covariance matrices to attain better performance. The AKF algorithm is solved similar to KF in three steps, i.e. initialization, prediction update and measurement update. The first step is similar to conventional KF. But the other two steps of conventional KF are modified using updating rules R1 and R2 which are as follows

Initialization:

The initial values of posteriori state estimate $(\hat{x}_0^+)$, posteriori state estimate error covariance matrix (P_0^+), and the initial process (Q_0) and measurement (R_0) covariance matrices are given as

$$\begin{aligned}
\hat{x}_0^+ &= E(\hat{x}_0) \ , \\
P_0^+ &= E[(x_0 - \hat{x}_0^+)(x_0 - \hat{x}_0^+)^T], \\
Q_0 &= \text{ diag } (q_{1,1},\ q_{2,2},\ q_{3,3}) \, , \\
R_0 &= \text{ diag } (v_{1,1},\ v_{2,2},\ v_{3,3}) \, ,
\end{aligned} \tag{35}$$

where $q_{i,i}$ and $v_{i,i}$ are the diagonal values of covariance matrices Q_0 and R_0 respectively.

R1- Measurement covariance update rule:

The adaptation of R_k is calculated with the measurement error update in Eq. (38), which uses the conventional time update step of KF equations given in (36) and (37), respectively.

$$\hat{x}_k^- = A(x_k)\hat{x}_{k-1} + B(x_k)u_{k-1}, \tag{36}$$
$$P_k^- = A(x_k)P_{k-1}A(x_k)^T + Q_{k-1}, \tag{37}$$
$$e_k = z_k - (C(x_k)\hat{x}_k^- + l(x_k)u_k + \Omega), \tag{38}$$
$$\alpha_1 = \frac{N_R - 1}{N_R}, \tag{39}$$
$$\bar{e}_k = \alpha_1 \bar{e}_{k-1} + \frac{1}{N_R} e_k, \tag{40}$$
$$\Delta R_k = \frac{1}{N_R - 1}(e_k - \bar{e}_k)(e_k - \bar{e}_k)^T - \frac{1}{N_R} C(x_k)P_k^- C(x_k)^T, \tag{41}$$
$$R_k = \mid diag(\alpha_1 R_{k-1} + \Delta R_k) \mid . \tag{42}$$

where $z^T = \begin{bmatrix} y_1 & y_2 & y_3 \end{bmatrix}$ is a vector of measured outputs.

R2- Process covariance update rule: For the adaptation of Q_k, we need to calculate the state estimation error in (46) by using the conventional KF design steps given in (43) to (45)

$$K_k = P_k^- C(x_k)^T (C(x_k)P_k^- C(x_k)^T + R_k)^{-1}, \tag{43}$$
$$\hat{x}_k = \hat{x}_k^- + K_k e_k, \tag{44}$$
$$P_k = (I - K_k C(x_k))P_k^-, \tag{45}$$
$$\hat{w}_k = \hat{x}_k - \hat{x}_k^-, \tag{46}$$
$$\alpha_2 = \frac{N_Q - 1}{N_Q}, \tag{47}$$
$$\bar{w}_k = \alpha_2 \bar{w}_{k-1} + \frac{1}{N_Q} \hat{w}_k, \tag{48}$$
$$\Delta Q_k = \frac{1}{N_Q}(P_k - A(x_k)P_k^- (A(x_k))^T) + \frac{1}{N_Q - 1}(\hat{w}_k - \bar{w}_k)(\hat{w}_k - \bar{w}_k)^T, \tag{49}$$
$$Q_k = \mid diag(\alpha_2 Q_{k-1} + \Delta Q_k) \mid . \tag{50}$$

The implementation of AKF has also been shown in Fig. 2 and results of AKF are discussed in Section 6.

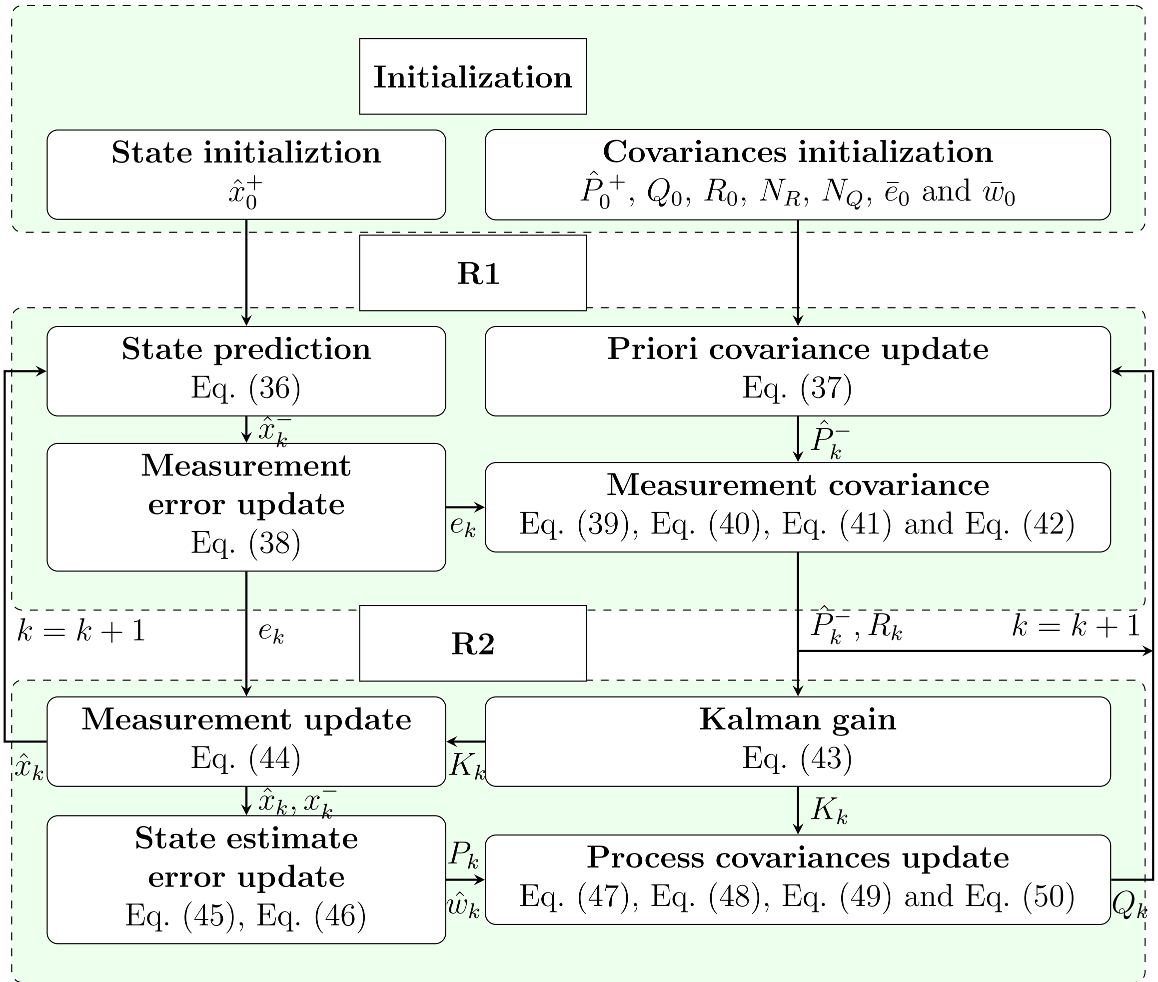

Figure 2: AKF implementation for robust estimation of BTS system.

6. Results and Discussions

In this section, the designed DSMC is implemented on the actual nonlinear model in the presence of external disturbances and noises. The implementation scheme is shown in Fig. 3. Moreover, the performance of DSMC is compared with PI controller. The practical scenario is presented by incorporating the following practical considerations.

- The noises given in (1) and (2) are considered during the simulation study to investigate their impact on the performance of the DSMC and

AKF. These noises are classified into the process noises, n_{p1}, n_{p2} and n_{p3}, and the measurement noises, n_{m1}, n_{m2} and n_{m3}, and they are generated by using the additive white Gaussian distribution. The process noises has zero mean and variance 1×10^{-4} and the measurement noises considered in (2) are represented by the following expressions

$$\begin{aligned} n_{m1} &\sim \mathcal{N}(0, 1.96), \\ n_{m2} &\sim \mathcal{N}(0, 4.62), \\ n_{m3} &\sim \mathcal{N}(0, 2.61 \times 10^{-4}). \end{aligned} \tag{51}$$

- The desired trajectories of the outputs are are selected based on the typical operating points of BTS given in, cf. [11].
- The gains of DSMC are selected as $N_1 = 0.007$,$N2 = 0.02$ and $N_3 = 0.05$. These gains are selected such that the bounds on the time derivatives of the control inputs, cf. (3) are satisfied.
- $\digamma_1 = 0.3$, $\digamma_2 = 0.05$ and $\mu = 0.7$ are choosen for the URED given in (9) and (10).
- The closed-loop system is solved by choosing a fixed step ode3 solver with a step size of 0.01 s.
- The structure used for PI controller is as follow

$$u_{PI_i} = K_{p_i} e_i(t) + K_{I_i} \int_0^t e_i(t) d\tau \tag{52}$$

where K_{p_i} and K_{I_i} are proportional and integral gains, respectively, $e_i = y_i - r_i$, $i \in \{1, 2, 3\}$ represents the tracking error for drum pressure, electric power and water level of the BTS, respectively. Moreover, the gains selected for PI controllers are $K_{p_1} = 0.07$, $K_{p_2} = 0.007$, $K_{p_3} = 1.7$, $K_{I_1} = 0.001$, $K_{I_2} = 0.001$ and $K_{I_3} = 0.01$.

The simulations are performed using MATLAB/Simulink. The results shown in Fig. 4 depict that the designed DSMC successfully tracks each output to their desired level in the presence of external disturbances and noises.

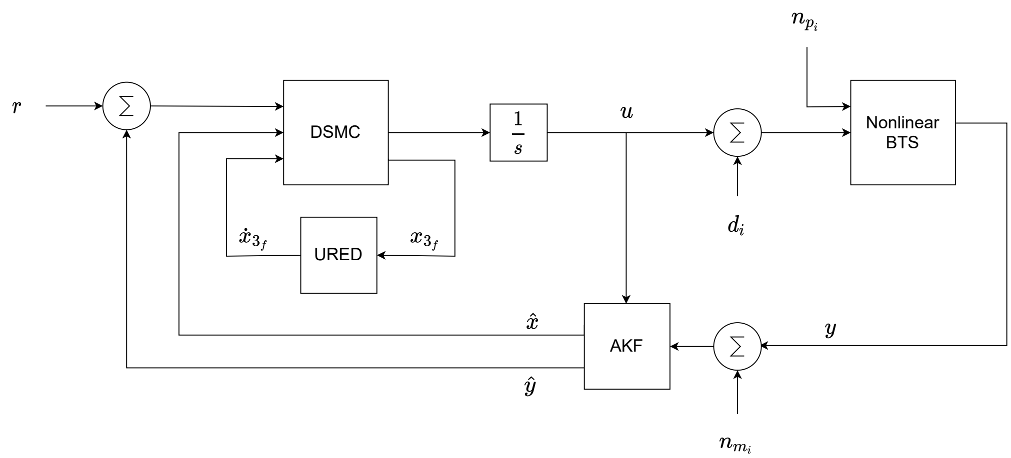

Figure 3: Implementation scheme for BTS control system.

It is pertinent to mention here that the filtered/estimated versions of the outputs have been used in the controller design because the measurements are noisy, cf. Fig. 7. The corresponding control efforts are also shown in Fig. 4. The disturbance rejection capability of DSMC is assessed by introducing input disturbances at 1.1 hr, and the profiles of disturbances are shown in Fig. 5. It is evident in Fig. 4 that the DSMC rejects the input disturbances by manipulating the control variables. Moreover, it maintains the control inputs within the allowed operating range. Hence, the designed DSMC exhibits adequate performance and robustness against the noises, external disturbance and modeling imperfections. It is worth observing that the designed control law does not exhibit the chattering phenomena, and the continuous control inputs are produced to achieve the desired control objectives. The time profiles of sliding variables and the tracking errors have been shown in Fig. 6. It can be seen that sliding mode is enforced in the manifold $\sigma_i = 0$ and $e_i \to 0$, where i=1,2,3.

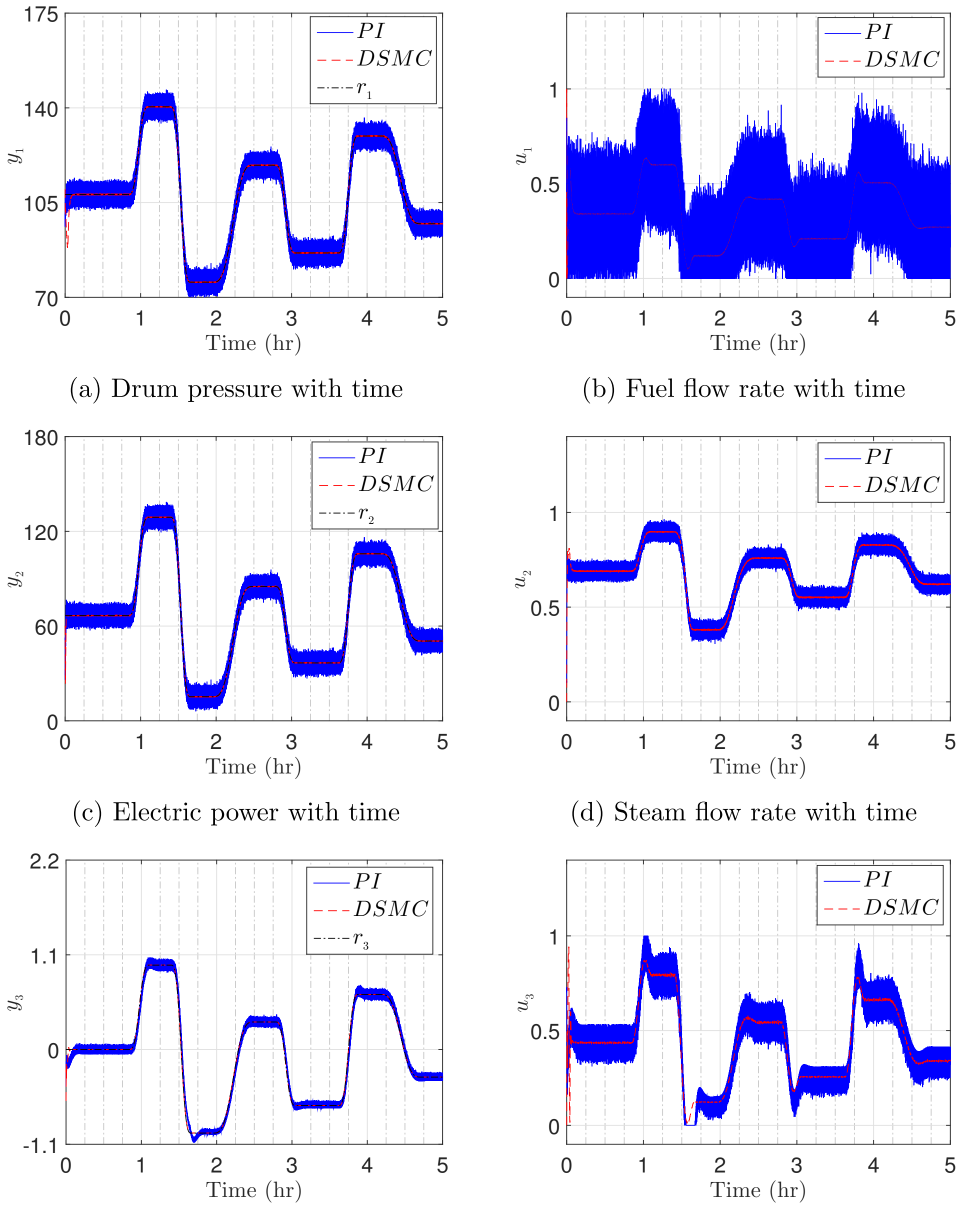

(a) Drum pressure with time

(b) Fuel flow rate with time

(c) Electric power with time

(d) Steam flow rate with time

(e) Water level with time

(f) Water flow rate with time

Figure 4: Outputs of the closed-loop and normalized control inputs with time

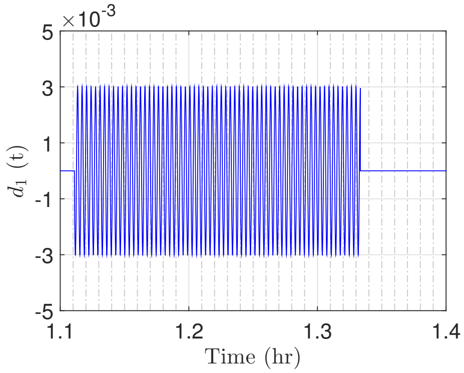

(a) d_1 with time

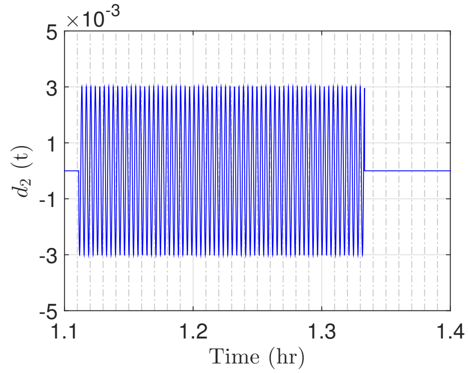

(b) d_2 with time

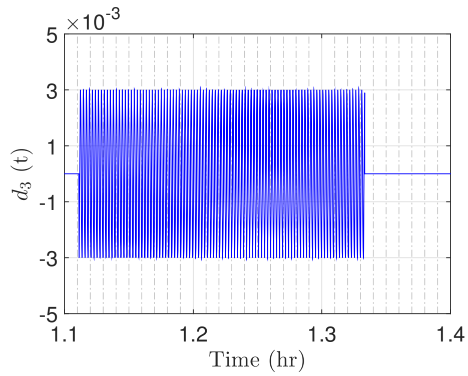

(c) d_3 with time

Figure 5: Input disturbances profile with time.

The effectiveness of DSMC is shown by making a quantitative analysis between DSMC and PI control scheme. The integral absolute error (IAE) is computed for both the control schemes which is as follow

$$\mathrm{IAE}_i = \int_0^{\infty} |e_i(t)| dt, \quad e_i(t) = y_i(t) - r_i(t), \tag{53}$$

where dt is the step size and the index $i \in \{1, 2, 3\}$ refers to the IAE value of the output i. Another criteria used for quantitative evaluation is the usage of the control energy. The average power for the control signals generated by the controllers is determined as

$$\mathrm{P}_{\mathrm{avg_j}} = \frac{1}{N} \sum_{k=1}^{N} u_j^2(k), \tag{54}$$

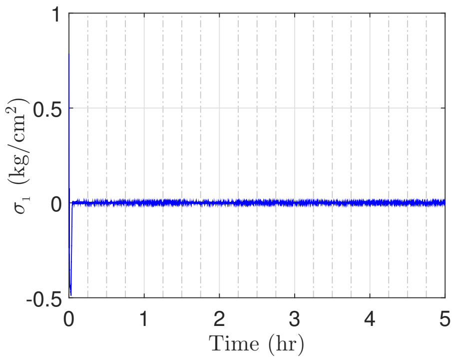

(a) σ_1 with time

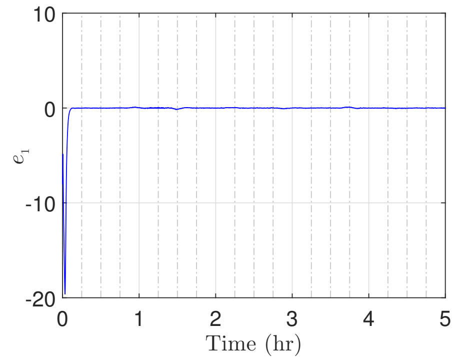

(b) e_1 with time

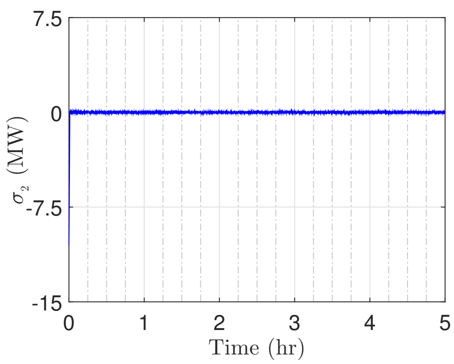

(c) σ_2 with time

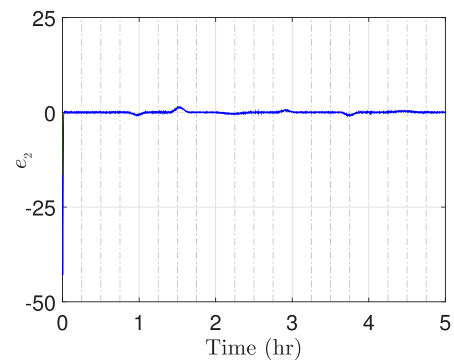

(d) e_2 with time

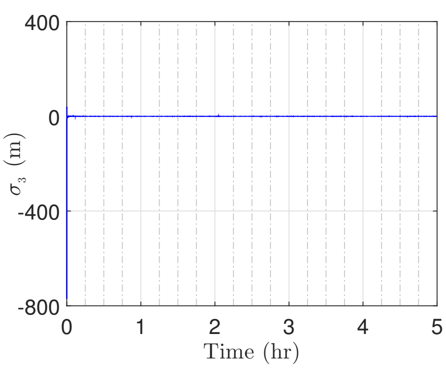

(e) σ_3 with time

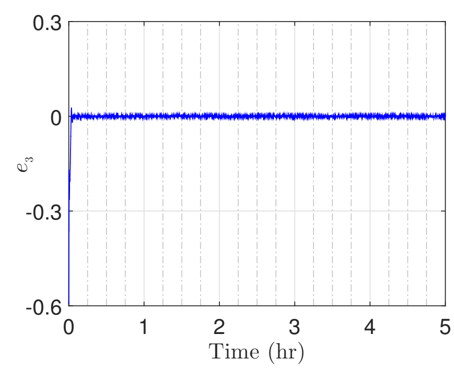

(f) e_3 with time

Figure 6: Sliding manifolds and tracking errors with time

where N is the number of samples and $j \in \{1, 2, 3\}$ is the index for the $\mathrm{P}_{\mathrm{avg}}$ of the control input j. The IAE and the $\mathrm{P}_{\mathrm{avg}}$ for both the control techniques are given in Table 4, which depicts that both the control techniques utilize almost same control energy, however, the performance of the DSMC is much better as compared to the PI controller.

Table 4: Comparison of PI and DSMC

Figure of Merit	**PI Controller**	**DSMC**
IAE_1	20701	4183.8
IAE_2	31712	4625.5
IAE_3	536.70	27.72
$\mathrm{P}_{\mathrm{avg}_1}$	0.1474	0.1379
$\mathrm{P}_{\mathrm{avg}_2}$	0.4747	0.4755
$\mathrm{P}_{\mathrm{avg}_3}$	0.2369	0.2339

The BTS and AKF are initialized with different initial conditions to evaluate the performance of the estimator. The designed parameters of AKF are summarized in Table 5. The performance of AKF is mainly dependent on tuning parameters N_R and N_Q. For noisy systems large values of N_R and N_Q are recommended as they give more weight to recursion (R_{k-1}, Q_{k-1}) than the current values ΔR_k and ΔQ_k during the adaptation of covariance matrices N_R and N_Q. Consequently, the AKF gain is smoothly changed through measurement error update (e_k) as given in (38) and state estimation error update ($\hat{w}_k$) in (46). Thus, in case, if the tracking is not satisfied then the gain will not converge to a small value. The performance of AKF is evaluated in terms of the root-mean-square error of the estimated state, i.e. x_3 which is defined as

$$\tilde{e}_{\mathrm{rms}} = \sqrt{\frac{1}{N}\sum_{i=1}^{N}\tilde{e}^2}, \;\; \tilde{e} = x_3 - \hat{x}_3, \tag{55}$$

where N are the number of samples. The computed $\tilde{e}_{\mathrm{rms}}$ value of x_3 is 0.1305 which indicates the accurate state reconstruction of BTS.

Table 5: Description of parameters

Symbol	**Value**
x_0	$[100\ 50\ 400]^T$
$\hat{x}_0^+$	$[110\ 60\ 390]^T$
$q_{i,i}$	10^{-5}
$v_{i,i}$	10^{-5}
w	10^{-4}
ν	4×10^{-4}
Q_0	$q_{i,i} \times \mathrm{I}_3$
R_0	$v_{i,i} \times \mathrm{diag}\ (10000\ 10000\ 10^{-1})$
N_R	7×10^{10}
N_Q	7×10^{10}
$\bar{e}_0$	$[1\ 1\ 1]^T$
$\bar{w}_0$	$10^{-4} \times [1\ 1\ 0.0001]^T$

The measured and estimated outputs are shown in Fig. 7, whereas, Fig. 8 shows the true and the estimated time profiles of the unknown state x_3. The results show that AKF yields smooth and accurate estimates of the outputs and the unknown state of BTS in the presence of process and measurement noises.

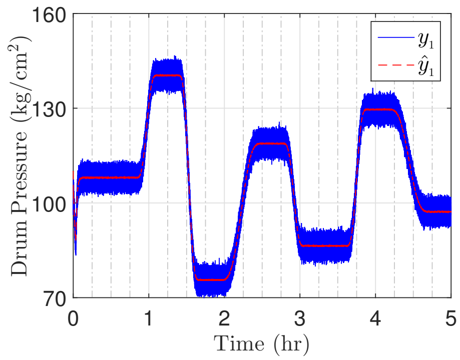

(a) Drum Pressure with time

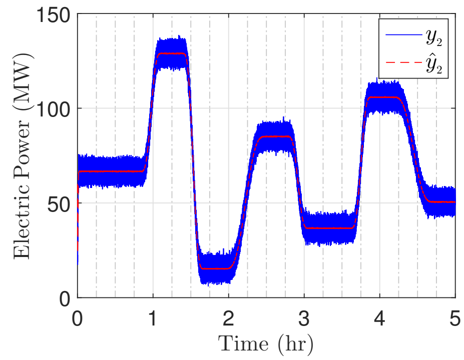

(b) Electric Power with time

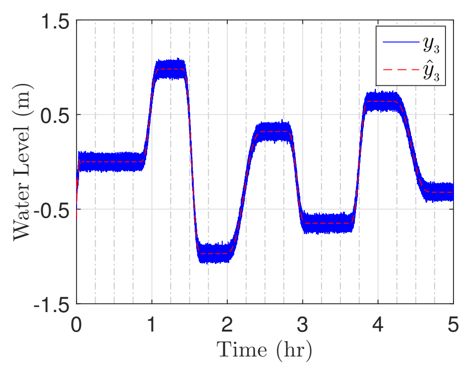

(c) Water Level with time

Figure 7: Measured outputs of BTS and their estimates with time.

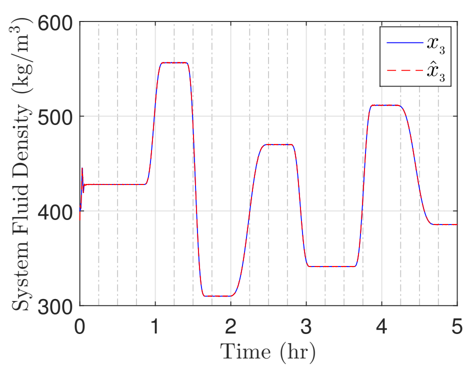

Figure 8: True and estimated time profiles of the unknown state (x_3) of BTS.

7. Conclusion

In this work, the significance of a multi-variable, model-based control system for the BTS is highlighted. A model-based DSMC control law has been designed to maintain the drum pressure, electric power and water level at the desired levels in the presence of modeling inaccuracies, external disturbances and noises. Owing to the complex mathematical expression of water level, the control problem is formulated by computing an auxiliary function and an implicit sliding manifold is designed such that the system fluid density tracks the auxiliary function. Subsequently, it has been shown that the designed control law ensures that the water level follows the desired level. The time derivative of the auxiliary function used in the control design is determined by employing URED. To make the control design possible, AKF has been designed to estimate the unknown system fluid density. The design of AKF is based on the quasi-linear decomposition of the BTS model. Moreover, the stability of the closed-loop system has been proved in the presence of external disturbances by using Lyapunov theory. The simulation results show that the proposed technique involving DSMC and AKF yields adequate performance in the presence of external disturbances, and measurement and process noises.

In the future, the current research work can be extended to a microgrid configuration in which the BTS can be integrated with other energy sources.

References

[1] T. Piraisoodi, M. W. Iruthayarajan, K. M. A. Kadhar, Application of single-and multi-objective evolutionary algorithms for optimal nonlinear controller design in boiler–turbine system, International Journal of Fuzzy Systems 20 (3) (2018) 803–816.

[2] W. Tan, H. J. Marquez, T. Chen, J. Liu, Analysis and control of a nonlinear boiler-turbine unit, Journal of process control 15 (8) (2005) 883–891.

[3] T. Piraisoodi, M. W. Iruthayarajan, K. M. A. Kadhar, An optimized nonlinear controller design for boiler–turbine system using evolutionary algorithms, IETE Journal of Research 64 (4) (2018) 451–462.

[4] B. Molloy, Modelling and predictive control of a drum-type boiler, Ph.D. thesis, Dublin City University (1997).

[5] X. Wu, J. Shen, Y. Li, K. Y. Lee, Data-driven modeling and predictive control for boiler–turbine unit, IEEE Transactions on Energy Conversion 28 (3) (2013) 470–481.

[6] Z.-g. Su, G. Zhao, J. Yang, Y.-g. Li, Disturbance rejection of nonlinear boiler-turbine unit using high-order sliding mode observer, IEEE Transactions on Systems, Man, and Cybernetics: Systems (2018).

[7] P.-C. Chen, J. S. Shamma, Gain-scheduled 1-optimal control for boiler-turbine dynamics with actuator saturation, Journal of process control 14 (3) (2004) 263–277.

[8] R. Dimeo, K. Y. Lee, Boiler-turbine control system design using a genetic algorithm, IEEE transactions on energy conversion 10 (4) (1995) 752–759.

[9] W. Tan, J. Liu, F. Fang, Y. Chen, Tuning of pid controllers for boiler-turbine units, ISA transactions 43 (4) (2004) 571–583.

[10] R. A. Maher, I. A. Mohammed, I. K. Ibraheem, State-space based h robust controller design for boiler-turbine system, Arabian Journal for Science and Engineering 37 (6) (2012) 1767–1776.

[11] K. Astrom, R. Bell, Dynamic models for boiler-turbine alternator units: Data logs and parameter estimation for a 160 mw unit, Department of Automation Control Lund Institute Technology Lund, Sweden Rep. LUTFD2/(TFRT-3192) (1987) 1–137.

[12] S. Ghabraei, H. Moradi, G. Vossoughi, Multivariable robust adaptive sliding mode control of an industrial boiler–turbine in the presence of modeling imprecisions and external disturbances: A comparison with type-i servo controller, ISA transactions 58 (2015) 398–408.

[13] S. Ghabraei, H. Moradi, G. Vossoughi, Design & application of adaptive variable structure & h robust optimal schemes in nonlinear control of boiler-turbine unit in the presence of various uncertainties, Energy 142 (2018) 1040–1056.

[14] H. Moradi, F. Bakhtiari-Nejad, M. Saffar-Avval, Robust control of an industrial boiler system; a comparison between two approaches: Sliding mode control & h technique, Energy Conversion and Management 50 (6) (2009) 1401–1410.

[15] H. Moradi, M. Saffar-Avval, F. Bakhtiari-Nejad, Sliding mode control of drum water level in an industrial boiler unit with time varying parameters: A comparison with h-robust control approach, Journal of Process Control 22 (10) (2012) 1844–1855.

[16] M. Ataei, R.-A. Hooshmand, S. G. Samani, A coordinated mimo control design for a power plant using improved sliding mode controller, ISA transactions 53 (2) (2014) 415–422.

[17] H. Moradi, G. Vossoughi, A. Alasty, Suppression of harmonic perturbations and bifurcation control in tracking objectives of a boiler–turbine unit in power grid, Nonlinear Dynamics 76 (3) (2014) 1693–1709.

[18] F. Fang, L. Wei, Backstepping-based nonlinear adaptive control for coal-fired utility boiler–turbine units, Applied Energy 88 (3) (2011) 814–824.

[19] D. Thangavelusamy, L. Ponnusamy, Elimination of chattering using fuzzy sliding mode controller for drum boiler turbine system, Journal of Control Engineering and Applied Informatics 15 (2) (2013) 78–85.

[20] M. Ławryńczuk, Nonlinear predictive control of a boiler-turbine unit: A state-space approach with successive on-line model linearisation and quadratic optimisation, ISA transactions 67 (2017) 476–495.

[21] L. Wang, Y. Cai, B. Ding, Robust model predictive control with bi-level optimization for boiler-turbine system, IEEE Access 9 (2021) 48244–48253.

[22] J. Zhu, X. Wu, J. Shen, Practical disturbance rejection control for boiler-turbine unit with input constraints, Applied Thermal Engineering 161 (2019) 114184.

[23] L. Pan, J. Shen, X. Wu, S. K. Nguang, C. Chen, Improved internal-model robust adaptive control with its application to coordinated control of usc boiler-turbine power units in flexible operations, International Journal of Systems Science 51 (4) (2020) 669–686.

[24] W. Tan, H. J. Marquez, T. Chen, Multivariable robust controller design for a boiler system, IEEE Transactions on Control Systems Technology 10 (5) (2002) 735–742.

[25] N. Yu, W. Ma, M. Su, Application of adaptive grey predictor based algorithm to boiler drum level control, Energy conversion and management 47 (18-19) (2006) 2999–3007.

[26] F. De Mello, Boiler models for system dynamic performance studies, IEEE Transactions on Power systems 6 (1) (1991) 66–74.

[27] J.-Z. Liu, S. Yan, D.-L. Zeng, Y. Hu, Y. Lv, A dynamic model used for controller design of a coal fired once-through boiler-turbine unit, Energy 93 (2015) 2069–2078.

[28] Y. M. Alsmadi, I. U. Rehman, A. Uppal A, V. Utkin, I. Chairez, M. Ibbini, Super-twisting-based sliding mode control of drum boiler energy conversion systems, International Journal of Control (2021) 1–10.

[29] B. Yang, M. Liu, H. Kim, X. Cui, Luenberger-sliding mode observer based fuzzy double loop integral sliding mode controller for electronic throttle valve, Journal of Process Control 61 (2018) 36–46.

[30] M. Liu, Z. Dong, Multiobjective robust h2/h fuzzy tracking control for thermal system of power plant, Journal of Process Control 70 (2018) 47–64.

[31] S. Spinelli, M. Farina, A. Ballarino, An optimal hierarchical control scheme for smart generation units: an application to combined steam and electricity generation, Journal of Process Control 94 (2020) 58–74.

[32] Y. Pan, Q. Li, H. Liang, H.-K. Lam, A novel mixed control approach for fuzzy systems via membership functions online learning policy, IEEE Transactions on Fuzzy Systems (2021).

[33] T. Jia, Y. Pan, H. Liang, H.-K. Lam, Event-based adaptive fixed-time fuzzy control for active vehicle suspension systems with time-varying displacement constraint, IEEE Transactions on Fuzzy Systems (2021).

[34] M. St-Pierre, D. Gingras, Comparison between the unscented kalman filter and the extended kalman filter for the position estimation module of an integrated navigation information system, in: IEEE Intelligent Vehicles Symposium, 2004, IEEE, 2004, pp. 831–835.

[35] A. UmaMageswari, J. J. Ignatious, R. Vinodha, A comparitive study of kalman filter, extended kalman filter and unscented kalman filter for harmonic analysis of the non-stationary signals, International Journal of Scientific & Engineering Research 3 (7) (2012) 1–9.

[36] N. Amor, S. Chebbi, Performance comparison of particle swarm optimization and extended kalman filter methods for tracking in non-linear dynamic systems, in: 2017 International Conference on Control, Automation and Diagnosis (ICCAD), IEEE, 2017, pp. 116–119.

[37] D. Wang, Y. Zhou, X. Li, A dynamic model used for controller design for fast cut back of coal-fired boiler-turbine plant, Energy 144 (2018) 526–534.

[38] C. Huang, X. Sheng, Data-driven model identification of boiler-turbine coupled process in 1000 mw ultra-supercritical unit by improved bird swarm algorithm, Energy 205 (2020) 118009.

[39] H. Fan, Z.-g. Su, P.-h. Wang, K. Y. Lee, A dynamic nonlinear model for a wide-load range operation of ultra-supercritical once-through boiler-turbine units, Energy 226 (2021) 120425.

[40] E. Cruz-Zavala, J. A. Moreno, L. M. Fridman, Uniform robust exact differentiator, IEEE Transactions on Automatic Control 56 (11) (2011) 2727–2733.

[41] V. Utkin, J. Guldner, M. Shijun, Sliding mode control in electro-mechanical systems, Vol. 34, CRC press, 1999.

[42] I. Hashlamon, K. Erbatur, An improved real-time adaptive kalman filter with recursive noise covariance updating rules, Turkish journal of electrical engineering & computer sciences 24 (2) (2016) 524–540.

[43] M. C. Teixeira, S. H. Zak, Stabilizing controller design for uncertain nonlinear systems using fuzzy models, IEEE Transactions on fuzzy systems 7 (2) (1999) 133–142.

[44] S. K. Godunov, A difference method for numerical calculation of discontinuous solutions of the equations of hydrodynamics, Matematicheskii Sbornik 89 (3) (1959) 271–306.